Cellular and Molecular Neurobiology (2021) 41:1727–1742
https://doi.org/10.1007/s10571-020-00942-y

ORIGINAL RESEARCH

Necroptotic–Apoptotic Regulation in an Endothelin-1 Model of Cerebral Ischemia

Chesarahmia Dojo Soeandy[1] · Andrew J. Elia[2,3] · Yanshan Cao[4] · Christopher Rodgers[1] · Shudi Huang[1] · Andrea C. Elia[1] · Jeffrey T. Henderson[1]

Received: 27 February 2020 / Accepted: 11 August 2020 / Published online: 25 August 2020

Abstract

The primary forms of cell death seen in ischemic stroke are of two major types: a necrotic/necroptotic form, and an apoptotic form that is frequently seen in penumbral regions of injury. Typically apoptotic versus necroptotic programmed cell death is described as competitive in nature, where necroptosis is often described as playing a backup role to apoptosis. In the present study, we examined the relationship between these two forms of cell death in a murine endothelin-1 model of ischemia–reperfusion injury in wildtype and caspase-3 null mice with and without addition of the pharmacologic RIPK1 phosphorylation inhibitor necrostatin-1. Analyses of ischemic brain injury were performed via both cellular and volumetric assessments, electron microscopy, TUNEL staining, activated caspase-3 and caspase-7 staining, as well as CD11b and F4/80 staining. Inhibition of caspase-3 or RIPK1 phosphorylation demonstrates significant neural protective effects which are non-additive and exhibit significant overlap in protected regions. Interestingly, morphologic analysis of the cortex demonstrates *reduced* apoptosis following RIPK1 inhibition. Consistent with this, RIPK1 inhibition reduces the levels of both caspase-3 and caspase-7 activation. Additionally, this protection appears independent of secondary inflammatory mediators. Together, these observations demonstrate that the necroptotic protein RIPK1 modifies caspase-3/-7 activity, ultimately resulting in decreased neuronal apoptosis. These findings thus modify the traditional exclusionary view of apoptotic/necroptotic signaling, revealing a new form of interaction between these dominant forms of cell death.

Keywords Murine models of stroke · Apoptosis · Necroptosis · Endothelin-1 · RIPK1 · Caspase-3

Introduction

Stroke affects more than fifteen million people worldwide every year and is the third leading cause of death in North America. The nature of stroke makes it a major source of serious long-term disability, with direct and indirect costs in the U.S.A. alone estimated at > $75 billion annually (World Health Organization 2004). Strokes can be broadly divided into two major categories: hemorrhagic and ischemic. Hemorrhagic strokes arise due to damage to endothelia ultimately resulting in leakage or rupture of cerebral vasculature. Despite being significantly more lethal on a per case basis, hemorrhagic strokes represent a minority of clinically observed strokes, with > 85% being embolic/ischemic in nature (Albers et al. 2016; Simonetti et al. 2013). Most often these arise as an ultimate consequence of progressive narrowing of cerebral vasculature which leads to blockage, vascular inflammation, or as a result of spontaneous embolic occlusion (Albers et al. 2016; Simonetti et al. 2013; World

✉ Jeffrey T. Henderson
jeff.henderson@utoronto.ca

1 Department of Pharmaceutical Sciences, University of Toronto, 144 College St. Rm 962, Toronto, ON M5S 3M2, Canada

2 Princess Margaret Cancer Center, University Health Network, 610 University Avenue Rm 7-323, Toronto, ON M5G 2C1, Canada

3 Department of Medical Biophysics, University of Toronto, 101 College Street Rm 15-701, Toronto, ON M5G 1L7, Canada

4 Department of Pharmaceutical Sciences, University of Toronto, 144 College St. Rm 1010, Toronto, ON M5S 3M2, Canada

Health Organization 2004). Although numerous candidate neuroprotective drugs have been examined in animal stroke models over the last few decades, only a minority have successfully progressed through stage III clinical trials (Cheng et al. 2004; Ford 2008; Ginsberg 2009). Indeed, current standards of care for ischemic stroke primarily focus on supportive measures aimed at vascular reperfusion—such as surgical intervention (endovascular thrombectomy) or administration of thrombolytics like tissue plasminogen activator—rather than approaches aimed at direct inhibition of neuronal death due to gaps in our understanding of ischemic programmed cell death (Del Zoppo et al. 2009).

The first 24-h period of ischemic stroke frequently involves two phases: the ischemic event and vascular reperfusion. These events trigger two morphologically distinct forms of neuronal cell death: a necrotic form, which is thought to occur in areas exposed to more prolonged and severe metabolic stress, and an apoptotic form, which can be found in interdigitating penumbral regions that are less severely affected (Broughton et al. 2009; Radak et al. 2017; Yuan 2009). Historically apoptosis was accepted to be the major form of programmed cell death in ischemia while necrosis was considered unregulated (Jun-Long et al. 2018; Vanlangenakker et al. 2008). More recent studies however have demonstrated that much of the necrotic cell death within the core of ischemic cortical injuries may be programmed—a form of cell death which has come to be known as *necroptosis* (Jun-Long et al. 2018; Vanlangenakker et al. 2008). Though necroptotic cells share many of the characteristics seen in those exhibiting necrosis, lysosomal rupture, organelle and cellular swelling, loss of membrane integrity (Alberts et al. 2008; Hitomi et al. 2008), necroptosis has been demonstrated to be a highly regulated process which is ATP-dependent, unlike necrosis (Jun-Long et al. 2018; Liu et al. 2018).

Necroptosis is typically induced by stimuli external to the cell which activate one or more members of the so-called Death Receptor (DRs) family which includes TNFR1, Fas, DR3, DR4/TRAILR1, DR5/TRAILR2, and DR6 (Han et al. 2011; Takahashi et al. 2012). Depending upon the nature of ligand binding, activation of these receptors ultimately promotes stable formation of either the Death-Inducing Signaling Complex (DISC, also known as complex II) or necrosome (complex IIb), which promotes the execution of apoptosis or necroptosis, respectively. Formation of the DISC promotes apoptosis through induction of activated caspase-8, which subsequently inhibits necroptosis via cleavage of RIPK1 and RIPK3 and activates downstream apoptotic executioners such as caspase-3 and caspase-7 by mechanism which typically involve Bid cleavage (tBid) (Feng et al. 2007; Galluzzi et al. 2018; Kruidering and Evan 2000; Lin et al. 1999; Nair et al. 2014; Schug et al. 2011). Alternatively in cases where levels of caspase-8 activity are reduced, the serine/threonine kinase RIPK1 will recruit and promote the activation of RIPK3 through formation of the necrosome. This in turn initiates RIPK3-mediated phosphorylation of MLKL at several sites to promote the formation of MLKL oligomers which translocate to the plasma membrane, resulting in membrane permeabilization (Cai et al. 2014; Han et al. 2011). As such, the interaction between necroptosis and apoptosis typically involves cross-pathway inhibition and mutual exclusivity.

In the present study, we sought to examine the nature of this interaction in a murine model of stroke. Previously, necroptosis has been shown to be involved in the mechanism of stroke injury in middle cerebral artery and bilateral common carotid artery stenosis models in which RIPK1 phosphorylation was inhibited using the small molecule inhibitor necrostatin-1 (Chen et al. 2018; Degterev et al. 2005; Zhang et al. 2016). However, a number of prior neuroprotective studies utilizing these models have failed to reproduce such findings in subsequent human clinical evaluations, and this has been attributed to a number of underlying deficiencies in the models used (Carmichael 2005; Ford 2008). Murine models that involve occlusion of large vascular territories often suffer from complications due to the stochastic nature of individual cerebral architecture (even in genetically identical mice), which contributes to its significant variability (Ghanavati et al. 2014). These models also typically demonstrate substantial injury size (21–45% of the affected hemisphere in MCAO) and result in significant subcortical injury, which are features not present for the great majority of human cortical strokes (for example, injury size typically spans 2–14% of the affected cortex) (Albers et al. 2016; Bacigaluppi et al. 2010; Carmichael 2005; Dulli et al. 1998; Pulli et al. 2012). These factors thus significantly complicate benefit analysis of any potential neuroprotective agent of human clinical stroke.

An alternative model that addresses many of the above problems involves the focal intracortical application of endothelin-1 (ET-1), a vasoactive peptide normally released during ischemic stroke which induces ischemic hypofusion for periods greater than 1 h (Macrae et al. 1993; Sapira et al. 2010; Soylu et al. 2012). While this approach has successfully been used to induce cortical ischemia in rats (Fuxe et al. 1992; Gilmour et al. 2004; Windle et al. 2006), results in murine strains have been mixed, generally demonstrating less cortical injury than that seen in rats (Horie et al. 2008; Roome et al. 2014; Soylu et al. 2012; Tennant and Jones 2009). In part this may be due to increases in the relative proportion of endothelin-B versus endothelin-A receptors in murine cerebral endothelial cells; thus promoting greater vasodilation versus vasoconstrictive effects, respectively, upon endothelin-1 stimulation compared to that seen in rats (Wiley and Davenport 2004). Previously, we have performed a detailed cellular and molecular characterization of this

model in mice and detailed the role of apoptosis in resulting injuries (Dojo Soeandy et al. 2019). In our current study, we build upon these findings characterizing the role of necroptosis in ischemia and its interaction with apoptotic signaling during the critical first 24-h period following ischemic induction. Work from prior CNS injury studies suggests that the execution of apoptosis versus necroptosis in the CNS operates via competitive mechanisms. However, analysis of the expression of apoptotic versus necroptotic markers in the CNS following injury have recently caused us to question this in stroke, leading us to hypothesize that there may exist cooperative interaction between these signaling pathways for this form of CNS injury in contrast to other forms of CNS injury. Analysis of genetic and pharmacologic inhibitors of these pathways during induction of endothelin-1-mediated end-arteriolar stroke reveals a surprising and previously uncharacterized cooperative regulatory interaction between necroptotic and apoptotic execution in CNS neurons. Consistent with this, inhibition of RIPK1 phosphorylation conferred similar levels of CNS protection to that seen following genetic loss of caspase-3 expression, with combinatorial necroptotic/apoptotic inhibition failing to yield additional significant neuroprotective benefit. Mechanistically, we demonstrate that inhibition of RIPK1 results in significant functional reductions in levels of activated caspase-3 and caspase-7 during the critical initial phase of programmed cell death involved in cerebral ischemia.

Methods

Animal Care and Stereotactic Surgery

All experimental procedures were performed in accordance with standards outlined by the Local Animal Care Committee and the University of Toronto, following the guidelines set by Ontario's Animal for Research Act and the federal Canadian Council on Animal Care. Animals were housed in a standard facility with twelve-hour light/dark cycle and unrestricted access to chow and water. Caspase-3 mutant mice were generated and maintained as described (Woo et al. 1998). Experiments were performed on 2- to 4-month-old wildtype (WT) CD1, C57Bl/6 J or caspase-3 null (C3KO) mice. Both male and female mice within each of the defined treatment groups were injected with vehicle or necrostatin-1 (35 µg/10 g, i.p.) twenty minutes prior to the administration of 2.5% Avertin (0.11–0.13 mL/10 g, i.p.) and administration of the analgesic Ketoprofen (0.05 mg/10 g, subcutaneous) at the start of surgery. Cortical area was prepared by removing a one-centimeter section of hair from the dorsal skull, sterilizing, and cutting a 0.8-cm incision along the midline between the lambda and bregma sutures. Surgery was performed as previously described (Dojo Soeandy et al. 2019). Briefly, surgeries were done on a standard Cunningham mouse stereotaxic instrument with temperature control over a period of 30 min. A 400 nl volume of 1 µg/µl endothelin-1 (R and D systems 1160) or vehicle was infused through a 100 µm O.D. pulled borosilicate glass capillary through 250 µm diameter holes at 3 cortical stereotactic sites: 2.0 mm lateral to the midline at 0.0, + 1.0, and + 2.0 mm relative to the bregma (anteroposterior-AP) at a depth of + 1.2 mm relative to the brain surface (dorsoventral-DV), targeting primary motor cortex and primary somatosensory areas of the lower limb and trunk. Upon closure of the overlying dermis using 6.0 polyurethane sutures, animals were placed in a recovery cage and maintained at 37 °C for 15 min prior to being moved to a monitored 25 °C recovery cage.

Electron Microscopy, Tissue preparation, and Histology

Electron Microscopy

At the indicated time-points, animals were perfused with 4% para-formaldehyde (PFA) and 0.1% glutaraldehyde in 100 mM cacodylate buffer at pH 7.4, at which time tissues were harvested and post-fixed with the same fixative overnight at 4 °C. As previously described (Dojo Soeandy et al. 2019; Sakai et al. 2000), dissected tissue elements were subsequently post-fixed in 1% osmium tetroxide for 2 h and embedded in Spurr resin. Subsequently, as described in (Dojo Soeandy et al. 2019; Pan et al. 2014, 2015; Sakai et al. 2000), samples were sectioned at 70 nm onto Formvar-coated 200 mesh copper grids, and stained with 2% uranyl acetate and 0.1% lead citrate. Imaging was performed using a Phillips CM 100 electron microscope.

Histology

Following tissue harvest, samples for histology and immunohistochemistry were fixed in 4% PFA in phosphate-buffered saline (PBS) at pH 7.4 for 15 min at room temperature followed by fixation at 4 °C overnight with agitation. Tissues were then dehydrated using an automated Tissue Tek VIP 3000 processor using a standard ethanol/xylene/wax incubation series and embedded in paraffin in the horizontal orientation. Tissues were sectioned through a minimum of 2 mm of tissue surrounding the primary region of interest at intervals of 147 µm (7 µm thickness) and subsequently fixed onto charged slides and bound to slides at 55 °C for a minimum of 3 h. For thionin staining, sections were dewaxed and rehydrated through a standard xylene/ethanol/water series and stained with 0.1% acidified thionin for 10 s followed by serial dehydration in ethanol/xylene and mounted with Permount (Fisher SP15-500).

Immunohistochemistry, Immunofluorescence, and TUNEL Assay

Peroxidase Immunohistochemistry

Sections were dewaxed and rehydrated as above, then incubated in 3% hydrogen peroxide for 15 min at room temperature with agitation to destroy endogenous peroxidase activity. Samples were then washed with PBS 2 × 5 min. Antigen retrieval was subsequently performed in 10 mM sodium citrate, pH 6.0 using a pressure cooker where a temperature of 100 °C was maintained for 10 min. Sections were then incubated in primary antisera (cleaved caspase-3, Cell signaling 9661s; cleaved caspase-7, Cell signaling 9491s; CD11b, Abcam ab133357; F4/80, Bio-Rad MCA497GAR) in histoblock solution containing 3% BSA, 20 mM $MgCl_2$, and 0.3% tween 20 in 10 mM PBS, pH 7.4, with additional 0.2% Triton-X-100 and 5% goat serum overnight at 4 °C. The next day, sections were washed for 5 min in 0.3% PBS-Tween 20, then 3 × 5 min in PBS. Sections were then incubated with appropriate biotinylated secondary antibody in PBS containing 0.2% Triton-X-100 for 1 h at room temperature with gentle agitation. Sections were then washed once in 0.3% PBS-T for 5 min, then PBS 3 × 5 min. Sections were incubated in avidin-HRP (ABC Vectastain Elite kit, Vector labs) according to the manufacturer's instructions for 1 h at room temperature with gentle agitation. Sections were then washed once in 0.3% PBS-T for 5 min and PBS 3 × 5 min, then developed using 3,3-diaminobenzidine (DAB peroxidase substrate kit, Vector labs) according to the manufacturer's instructions. Sections were counterstained with hematoxylin for 2 min and differentiated in acidic alcohol (70% ethanol, 1% HCl) before neutralization in ammonium hydroxide, followed by dehydration and mounting in Permount as previously described (Dojo Soeandy et al. 2019).

Immunofluorescence

Following section rehydration and antigen retrieval as given above, sections were incubated with RIPK1 (BD Bioscience 610458) and cleaved caspase-3 (Cell Signaling 9661s) at a 1:250 dilution in 0.3% tween-20 PBS and 5% goat serum overnight at 4 °C. The following day sections were washed 3 × 5 min in 0.3% PBS-T/5% goat serum and incubated in anti-mouse Alexa 594/anti-rabbit Alexa 488 (Invitrogen A11032 and A11008, respectively) in 0.3% PBS-T for 2 h at 4 °C at a dilution of 1:400. Sections were then washed 3 × 5 min in PBS, PBS-T, PBS, followed by mounting and imaging.

TUNEL Staining

As previously described (Dojo Soeandy et al. 2019), staining was performed following rehydration of tissues and subsequent permeabilization with 20 µg/ml Proteinase K (Bioshop PRK403.100) in 10 mM Tris pH 7.5 at 37 °C for 17 min. Slides were then washed 3 × 5 min in PBS and stained with FITC-labeled TUNEL reagent according to the manufacturer's instructions (Roche Diagnostics 11684795910) for 1.5 h at 37 °C. Sections were then washed in PBS 3 × 5 min with a final wash in 10 mM Tris–HCl, pH 7.5 for 5 min. Sections were wet-mounted and imaged.

Image Analysis and Statistics

Thionin and immunohistochemical slides were digitally scanned using Hamamatsu NanoZoomer 2.0 HT scanner. Region of interest (ROI) measurements and cellular quantitation of thionin and peroxidase-stained sections were performed using NanoZoomer's Digital Pathology software. Total lesion volumes were determined from a sum of thionin-stained sections obtained at intervals of 147 µm multiplied by the lesion area observed for each slide. Cellular quantitation of thionin and peroxidase-stained sections were done within a 500 µm radius from ET-1 infusion site. Specifically, intact cellular profiles were determined using thionin-stained samples based on neural cell diameter of 10–20 µm. Analyses of data were blinded with respect to treatment groups. No significant differences in the distribution and extent of neuroprotection were observed between male and female specimens within specified genotype or pharmacologic treatment classes. As such results are reported for aggregate male and female data. Fluorescent imaging of stained sections was done using a Nikon E1000R motorized microscope equipped with appropriate DAPI, FITC, TRITC, and Cy5/DiD excitation/emission filters. Statistical comparison of 2 groups was performed using standard student's *t* test (unpaired, two tailed with assumption of equal variance) with significance between groups determined at a minimum level of $p < 0.05$. Statistical analyses of greater than 2 groups with one independent variable were performed using one-way ANOVA and Tukey's post hoc with significance defined at a minimum level of $p < 0.05$. Statistical measures were performed using Microsoft Excel and Graphpad Prism 6 software.

Results

Inhibition of RIPK1 Kinase Activity is Protective Against Acute Cell Death Induced by Endothelin-1 and is Non-additive to Protective Effects Observed by Loss of Caspase-3

Previously, we have detailed properties of an end-arteriolar ischemic/reperfusion model through stereotactic infusion of endothelin-1 (ET-1), demonstrating the presence of caspase-3-dependent apoptosis in this model (Dojo Soeandy et al. 2019). Similar to what we observed previously, stereotactic application of ET-1 in wildtype (WT) mice resulted in a substantial increase in the region of cortical injury compared to that seen following infusion of vehicle alone (Fig. 1a). By contrast, application of the RIPK1 inhibitor necrostatin-1 (Nec-1) results in a reduction in the degree of cortical injury compared to that seen with ET-1 alone as observed by both thionin staining and

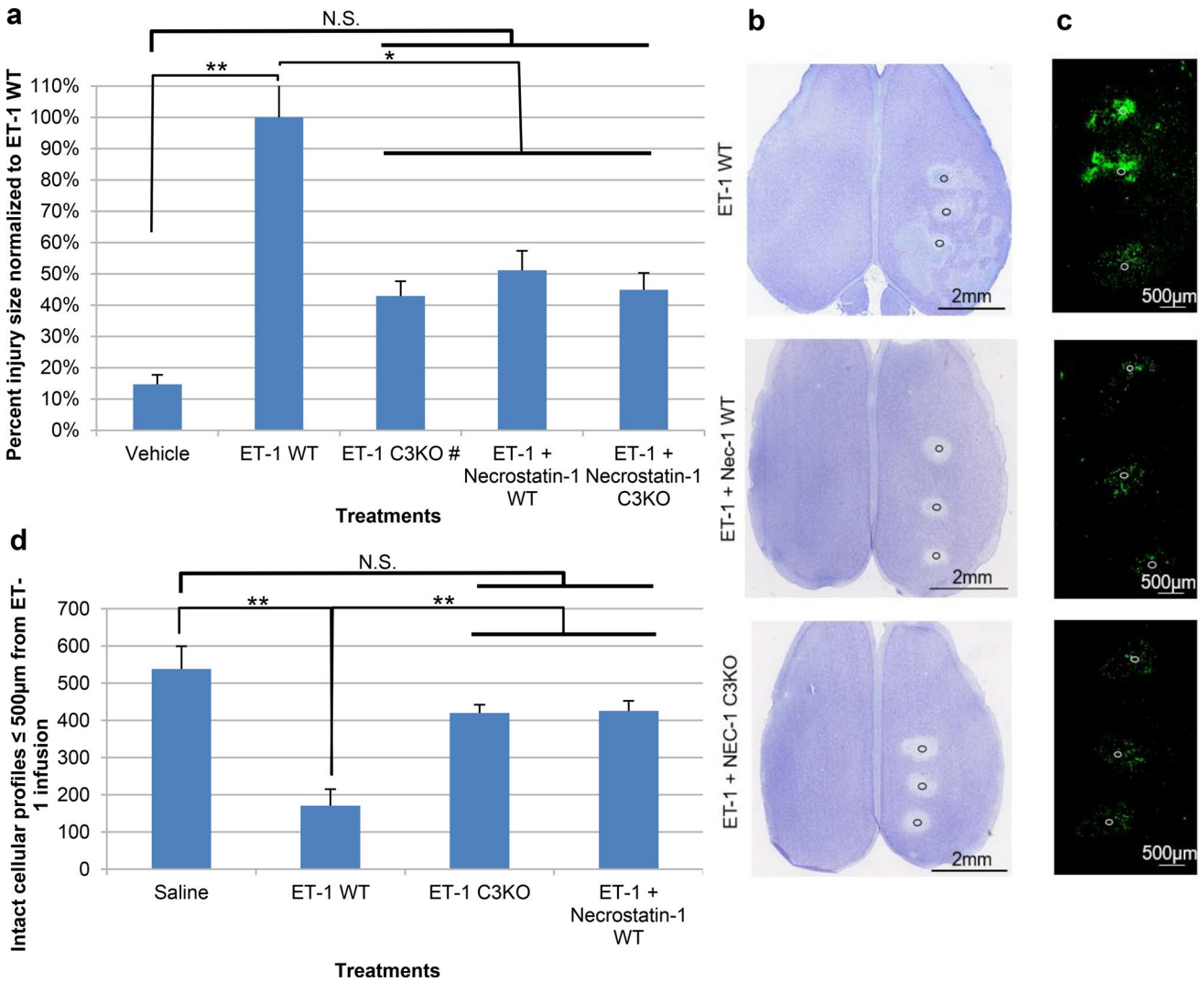

Fig. 1 Effect of RIP1 and caspase-3 inhibition on endothelin-1-induced ischemic injury 24 h post treatment. **a** Quantitative analysis demonstrating average percent injury size normalized to ET-1 WT ± S.E.M. ($n = 6$, 8, 6#, 8, 8, respectively). # Represents volumetric results from experimental set previously published (Dojo Soeandy et al. 2019), i.e., ET-1 C3KO. Demonstrated are representative horizontal overviews of dorsal cortices at the level of cortical layer III stained with thionin (**b**) and TUNEL (**c**) for endothelin-1 (ET-1)-treated wildtype (WT), wildtypes additionally exposed to necrostatin-1 (Nec-1), and Nec-1-exposed caspase-3 null (C3KO) mice. Relative position of injection sites are noted by the circles. **d** Average counts of intact cellular profiles (with 10–20 μm cell diameter) ≤ 500 μm from ET-1 infusion site as per thionin staining. Data represented as mean ± S.E.M. ($n = 9$, 18, 12, 12). Significance was determined using a one-way ANOVA with Tukey's Post hoc for both **a** and **d;** F (4, 31) = 7.121, $p < 0.0005$ for **a** and F (3, 47) = 11.28, $p < 0.0001$ for **d**. *Represents statistically significant difference at $p < 0.05$, **represents statistically significant difference at $p < 0.01$. *N.S.* no statistical significance

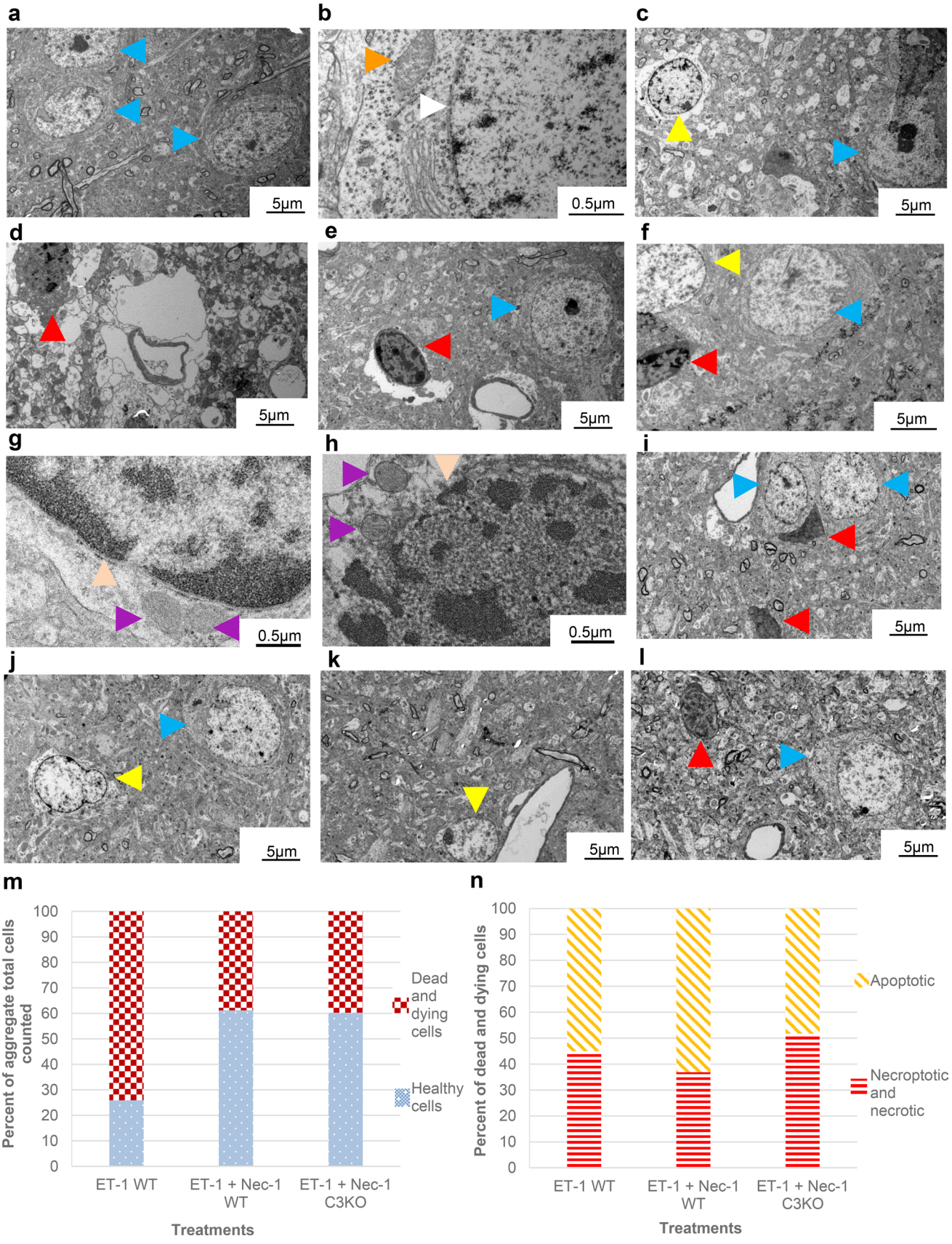
a
b
c
d
e
f
g
h
i
j
k
l
5μm
0.5μm
m
Percent of aggregate total cells counted
100
90
80
70
60
50
40
30
20
10
0
ET-1 WT
ET-1 + Nec-1 WT
ET-1 + Nec-1 C3KO
Treatments
Dead and dying cells
Healthy cells
n
Percent of dead and dying cells
Apoptotic
Necroptotic and necrotic

◂**Fig. 2** Electron microscopy of cortical (layer V) neuron morphology 24 h following ET-1 treatment into the cortex and the effect of RIP1 inhibition and loss of caspase-3. Few dying neurons are observed in contralateral cortices not exposed to ET-1 (**a**, **b**) Blue arrowheads highlight healthy neurons with intact nuclear membrane (white arrowhead) and mitochondria (orange). **c–f** ET-1 treatment in WT mice induces neurons with apoptotic morphology (yellow arrowheads) or necrotic/necroptotic morphology (red arrowheads) with few healthy neurons (blue arrowheads); **c**, **d** Regions proximal to site of endothelin-1 infusion; **e**, **f** Regions more distal to ET-1 infusion. **g** Higher magnification view of apoptotic cells demonstrating chromatin condensation with intact nuclear membrane (peach arrowhead) and mitochondrial dissolution (purple arrowhead). **h** Higher magnification view of necrotic/necroptotic cell showing loss of nuclear integrity (peach arrowhead) and mitochondrial swelling (purple arrowhead). **i**, **j** Dying neurons in Nec-1-treated wildtype mice. **k**, **l** Affected cortical neurons in Nec-1-treated caspase-3 null mice. For **i–l** blue arrowhead denotes intact neurons, yellow—apoptotic and red—necroptotic cells. Scale bars as indicated. **m** Percent aggregate cell counts demonstrating healthy vs. injured cellular morphologies ($n = 54$, 49, 73). **n** Frequency of apoptotic vs. necroptotic/necrotic phenotypes as a function of treatment group

TUNEL DNA end-labeling (Fig. 1a–c). In order to better understand the mechanism of these effects, we first determined the relative volume of cortical injury, observing that application of Nec-1 resulted in approximately a 50% decrease in the volume of injury compared to ET-1 alone. Given that this reduction is similar in magnitude to that seen following ablation of the executioner caspase caspase-3 (Fig. 1a C3KO), we examined the effect of combinatorial inhibition through the application of necrostatin-1 in caspase-3 null mice. As shown in Fig. 1a, b, the volume of injury observed in the combinatorial treatment group (Nec-1-treated caspase-3 null mice) was comparable to that seen in caspase-3 KO alone and Nec-1-treated wildtypes, demonstrating that during the immediate (24 h) period following injury combinatorial inhibition of caspase-3 and RIPK1 does not provide further significant protection to the ischemic cortex. To further investigate this, TUNEL staining was performed on cortical sections. As shown in Fig. 1b, application of necrostatin-1 notably reduces tissue loss within secondary regions of injury. As shown in Fig. 1c, Nec-1 application also substantially reduced numbers of TUNEL-positive cells, an effect which is not further diminished upon ablation of caspase-3. To further confirm this at the cellular level, we ascertained numbers of intact neuronal profiles based on cell diameter within 500 microns of the epicenters of endothelin-1 infusion in layer V of affected cortices. As shown in Fig. 1d, 24 h post infusion ET-1-treated wildtype animals exhibited an approximately 70% loss of neurons compared with a ~ 22% reduction seen in caspase-3 null and necrostatin-1-treated animals. The similarity of the neuronal loss and reduction in TUNEL-positive cells seen in caspase-3 null and Nec-1-treated animals suggests that, in contrast to the current competitive model of apoptotic versus necroptotic activation, RIPK1 and caspase-3 programmed cell death may be linked.

RIPK1 Inhibition Reduces the Appearance of Neurons with Apoptotic Morphology

In order to gain greater insight into the relationship between RIPK1 and caspase-3-mediated cell death, we examined the ultrastructure of dying neurons within layer V of the ischemic cortex by electron microscopy (EM) (Fig. 2a–n). Consistent with our previous observations, exposure of cortical neurons to endothelin-1 results in a significant rise in cell death compared to that seen in comparable regions of the contralateral cortex (viable neurons-blue arrowheads, Fig. 2a–h). In wildtype animals, infusion of endothelin-1 resulted in cell death for more than 70% of cells examined (Fig. c–h, m). The phenotype observed in dying cells was approximately equally divided between those displaying an apoptotic phenotype (Fig. 2c, f, g, n; yellow) and those displaying necrotic features (Fig. 2d–f, h, n; red). Though total numbers of cell death observed between these phenotypes were approximately equal within the zone examined (0-500 µm from ET-1 infusion site), the distribution of cells displaying necrotic features was elevated in regions more proximal to the site of ET-1 infusion (Fig. 2c, d), while more distal regions commonly exhibited a greater occurrence of apoptotic cells (Fig. 2e, f). Treatment with necrostatin-1 in ET-1-treated animals resulted in a reduction in total cell death within cortical layer V compared to endothelin-1 alone (Fig. 2i, j, m), affecting both apoptotic and necroptotic cell death with somewhat greater effects on necroptotic populations (Fig. 2i, j, n). By contrast ET-1 treatment in caspase-3 null mice also resulted in a reduction in overall cell death (Fig. 2k–m) in which the distribution of death was comparable between apoptotic and necroptotic phenotypes (Fig. 2k, l, n).

Inhibition of RIPK1 Phosphorylation Reduces Numbers of Neurons Expressing Activated Caspase-3 and Activated Caspase-7 24 h Following Endothelin-1 Infusion

To further characterize the link between RIPK1-mediated cell death and apoptosis in ischemic–reperfusion injury, the state of the two principle executioner caspases (caspase-3 and caspase-7) was examined. As shown in Fig. 3a, active (cleaved) caspase-3 is not detected in the healthy (contralateral) cortex, whereas exposure to endothelin-1 results in a significant increase in the number of neurons expressing active caspase-3 (Fig. 3b). Consistent with TUNEL, volumetric and cellular ultrastructural findings described above, application of Nec-1 lead to a substantial reduction in the numbers of neurons expressing active

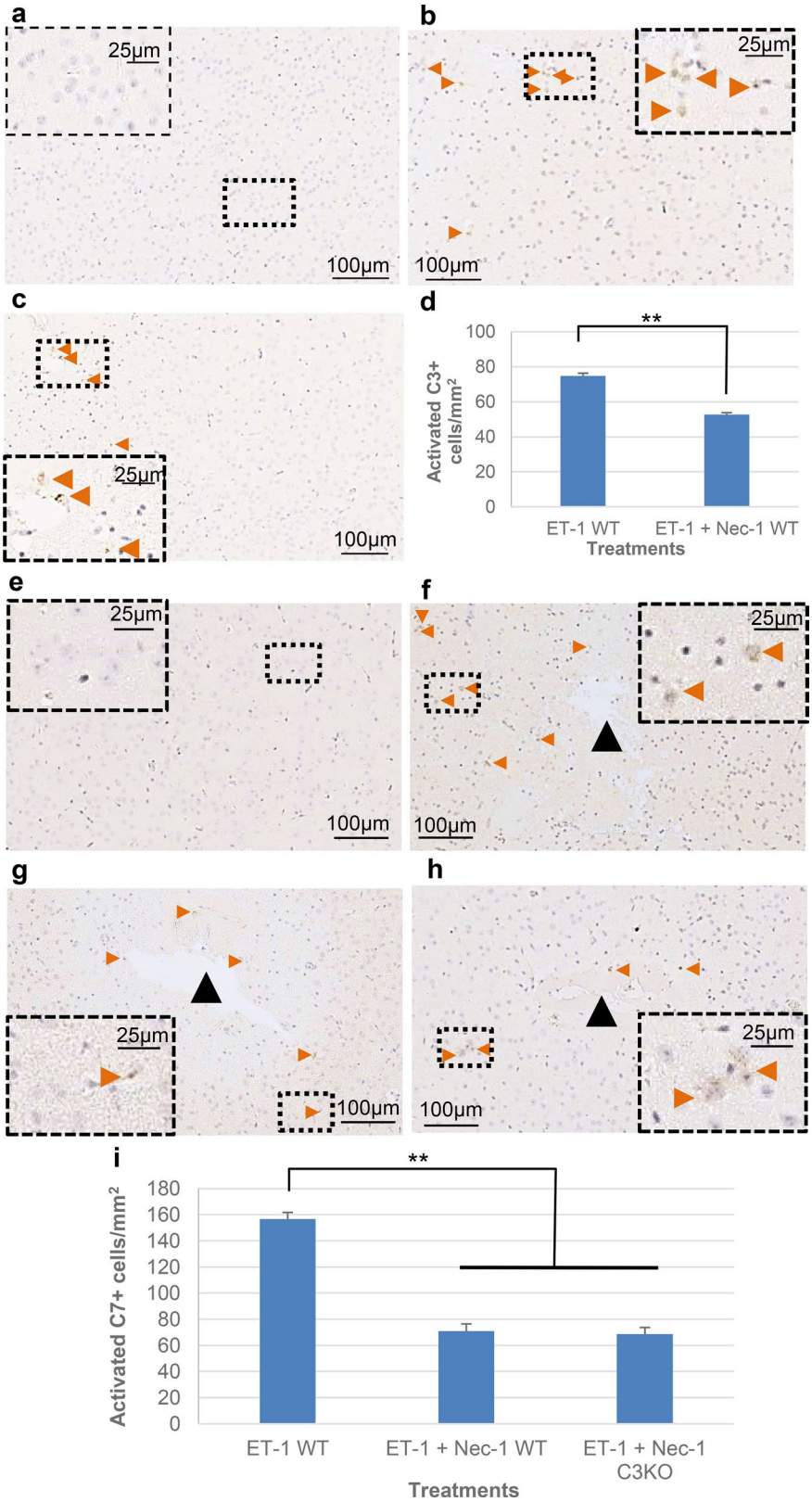

Fig. 3 RIPK1 effect on caspase-3/-7 activation in cortex 24 h following endothelin-1 infusion. Shown are horizontal (layer III) sections. **a–d** Caspase-3 activation 24 h after necrostatin-1 treatment in wildtype and caspase-3 null mice. **a** Activated caspase-3 staining in contralateral cortex without endothelin-1 treatment. **b** Activated caspase-3 staining in the cortex of WT mice exposed to ET-1. **c** Activated caspase-3 staining in ET-1 + Nec-1-treated wildtype mice. Peroxidase-stained caspase-3-positive cells are indicated by orange arrowheads in each case. Scale bars as indicated. **d** Analysis of activated caspase-3-positive cells/mm^2. Data represented as mean ± S.E.M. ($n = 6$) with significance determined by standard student t test (unpaired, two tailed t test, assumption of equal variance). **Represents statistical significance at $p < 0.01$. **e–i** Caspase-7 activation 24 h after necrostatin-1 treatment in wildtype and caspase-3 null mice. **e** Caspase-7 staining in contralateral cortex without endothelin-1 treatment. **f–h** Caspase-7 activation in endothelin-1-treated wildtype (**f**), Nec-1-treated wildtypes (**g**), and Nec-1-treated caspase-3 null mice (**h**). Black arrowheads highlight site of endothelin-1 infusion. Activated caspase-7-positive cells are indicated by orange arrowheads. Scale bars as indicated. **i** Analysis of cleaved caspase-7-positive cells/mm^2. Data represented as mean ± S.E.M. ($n = 6$), significance determined using a one-way ANOVA with Tukey's Post hoc (F (2, 15) = 75.96, $p < 0.0001$). **Statistically significant at $p < 0.01$

caspase-3 (Fig. 3c, d). Similar to caspase-3, examination of cortices for their expression of caspase-7 revealed an absence of active caspase-7 in unlesioned cortex (Fig. 3e), with significant increases in activated caspase-7 following endothelin-1 treatment (Fig. 3f). Analogous to the findings observed for activated caspase-3, treatment with

necrostatin-1 (in both the presence and absence of functional caspase-3) led to a decrease in number of neurons expressing activated caspase-7 (Fig. 3g–i). Thus, inhibition of RIPK1 kinase activity appears to functionally inhibit activation of both caspase-3 and caspase-7 in the ischemic cortex.

To further investigate the mechanism of this effect, we examined cellular expression of RIPK1 and activated caspase-3 in ischemic cortical injury. As shown in Fig. 4a, $RIPK1^+$ neurons exhibit a strong gradient of diffusion proximal to sites of ET-1 infusion. Analysis of caspase-3^+/$RIPK1^+$ double-positive cells demonstrates that this population represents $27 \pm 5\%$ of total $RIPK1^+$ cells for the time examined in wildtypes as shown in Fig. 4b, c (yellow cells). The greater abundance of $RIPK1^+$ cells compared to activated caspase-3 may indicate a downstream role for caspase-3 activation. Nec-1 treatment reduces the frequency of $RIPK1^+$ cells, resulting in apparent enhancement of the frequency of double-positive cells (Fig. 4b, d). Genetic ablation of caspase-3 on the other hand does not prevent the appearance of $RIPK1^+$ cells (Fig. 4e), consistent with the role of RIPK1 upstream of caspase-3.

Inhibition of RIPK1 Kinase Activity Does not Alter Levels of Granulocyte Infiltration or Microglia Activation

To determine if the effects observed following inhibition of RIPK1 kinase activity might arise as a result of secondary cellular changes such as granulocyte infiltration or microglia activation during the first 24 h following the induction of ischemia, these measures were examined. To screen broadly, sections were stained for CD11b to identify populations of granulocytes, monocyte/macrophages and microglia, and stained for F4/80 to further demarcate macrophages and microglia. As shown in Fig. 5a, b, though generalized staining of microglial processes can be observed even within the hemisphere contralateral to injury, a noted increase in granular non-process-bearing CD11b staining is observed proximal to sites of ET-1 infusion (black arrowhead) consistent with granulocyte infiltration. Treatment with necrostatin-1 in either wildtype or caspase-3 knockouts demonstrated no significant alteration in the extent or distribution of granulocytes compared to ET-1 alone (Fig. 5b–e).

Staining with F4/80 demonstrated a diffuse presence of microglia and monocyte/macrophages in the region surrounding ET-1 infusion site at 24 h following injury compared to comparable sites in the contralateral cortex (Fig. 6a, b). Similar to results obtained with CD11b, no significant difference was observed following necrostatin-1 treatment in wildtype or caspase-3 null mice compared to that seen in ET-1-treated wildtypes (Fig. 6b–e).

Discussion

As noted in previous studies, early signaling events critically regulate the ultimate nature and extent of neuronal cell death observed in the CNS during stroke (Heiss 2010; McCabe et al. 2009; Meng et al. 2004; Raghupathi 2004; Raghupathi et al. 2000; Symon 1987). Thus, a key consideration in the development of therapeutic strategies aimed at protecting at-risk ischemic tissue is to identify and target those mechanisms regulating the downstream progression of cell death at the affected neural loci. Numerous studies have demonstrated that both apoptosis and necroptosis play major roles in the early ischemic cell death observed (Degterev et al. 2005; Deng et al. 2019; Le et al. 2002; Sun et al. 2015; Zgavc et al. 2012). Using an endarteriolar ischemic–reperfusion model involving stereotactic intracortical infusion of endothelin-1 as previously described (Dojo Soeandy et al. 2019), we examined those cell signaling events occurring during the critical initial 24-h period following ischemia due to its dominant role in neuronal death and the initiation of secondary events such as tissue inflammation and phagocytosis (Heiss 2010; McCabe et al. 2009; Meng et al. 2004; Raghupathi 2004; Raghupathi et al. 2000; Symon 1987). Having previously examined the role of apoptosis in this model, we sought to further determine the role of necroptosis in this model and the relationship between apoptosis and necroptosis in ischemic–reperfusion injury (Dojo Soeandy et al. 2019).

Similar to previous observations following middle cerebral artery occlusion, we observe that treatment with necrostatin-1 results in a significant protective effect within the ischemic cortex (Degterev et al. 2005; Deng et al. 2019; Xu et al. 2010). Previously, these findings have been interpreted on the cellular level as arising from a mutually suppressive competitive interaction between the execution of apoptosis versus necroptosis, in which one signaling system or the other ultimately dominates, resulting in suppression of the alternative pathway in each cell. According to this view, the protective effects seen in ischemic neurons following inhibition of RIPK1 serine/threonine kinase activity arise solely through inhibition of the process of necroptosis. Thus, combinatorial inhibition of both apoptosis *and* necroptosis under these conditions should result in the rescue of two distinct populations of ischemic neural cells (Degterev et al. 2005; Deng et al. 2019; Xu et al. 2010). By contrast, our detailed molecular and ultrastructure examination of neuronal cell death response following endothelin-1 induced ischemia does not support this population response. This is understandable in retrospect given that these studies either have not directly examined levels of apoptotic versus necroptotic execution in parallel, or have relied upon the use

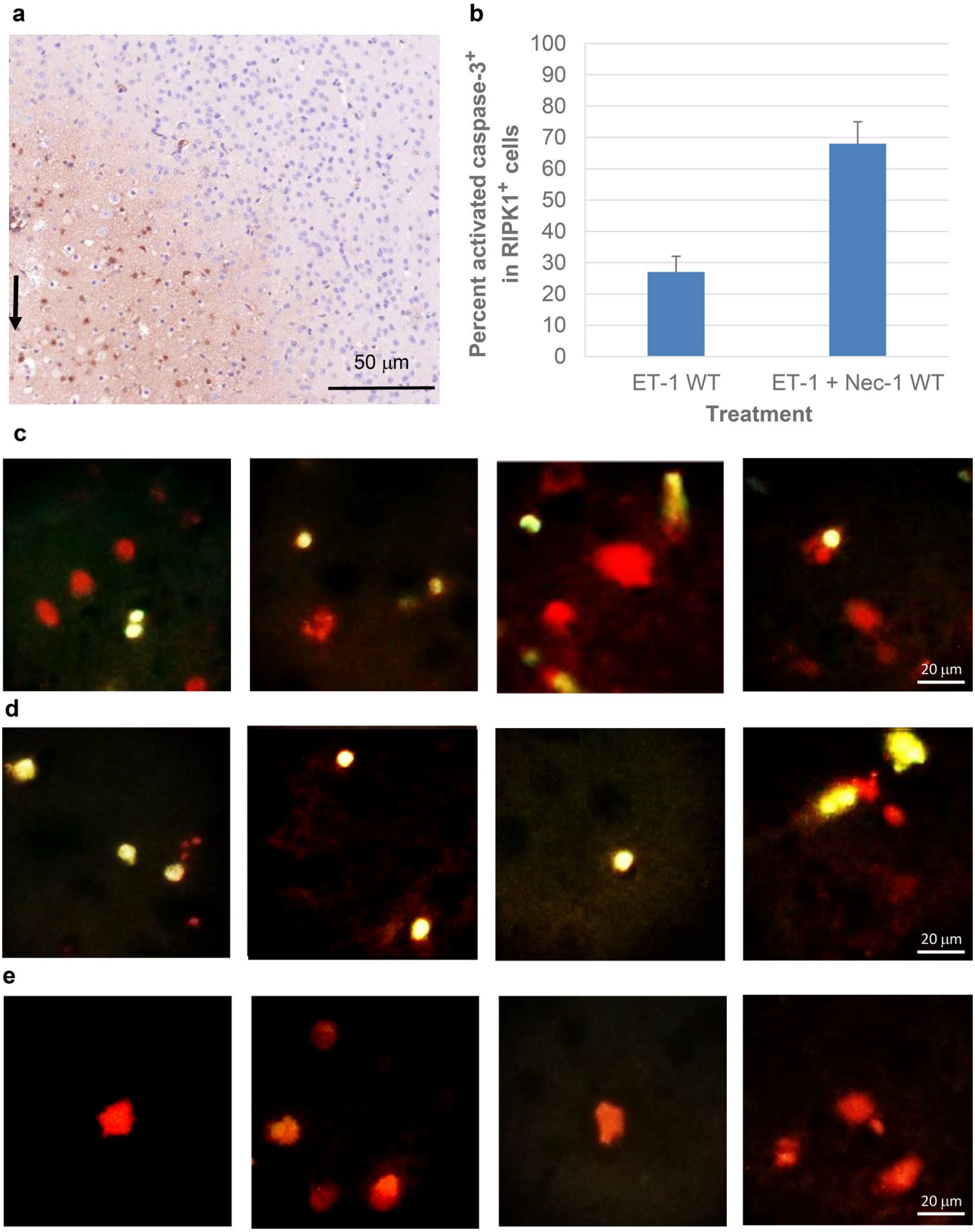
a
50 μm
b
Percent activated caspase-3+ in RIPK1+ cells
100
90
80
70
60
50
40
30
20
10
0
ET-1 WT
ET-1 + Nec-1 WT
Treatment
c
20 μm
d
20 μm
e
20 μm

◂**Fig. 4** RIPK1/activated caspase-3 co-distribution within the cortex 24 h following endothelin-1 treatment. **a** Distribution of RIPK1-positive cells within ET-1-treated cortex. Black arrow indicates the site of endothelin-1 infusion. **b** Percent double-positive activated caspase-3/RIPK1 cells as a function of treatment group. Data represented as mean ± S.E.M. ($n = 9$). **c–e** Examples of cell staining observed ≤ 500 µm from ET-1 infusion site; RIPK1 (red), and RIPK1/activated caspase-3 (yellow) cells are shown. **c** Immunofluorescent staining of WT mice treated with ET-1; **d** WT mice treated with ET-1 and Nec-1; **e** C3KO mice treated with ET-1 and Nec-1. Scale bars as indicated

of peptidic inhibitors such as the pan-caspase inhibitor such as z-VAD-fmk or anti-apoptotic polypeptides such as Gly(14)-humanin (HNG) to determine apoptotic contributions to injury (Degterev et al. 2005; Deng et al. 2019; Xu et al. 2010). This has been observed to be problematic, as we and others have shown using both gene knockouts and biochemical approaches that such inhibitors suffer from several limitations including a lack of absolute target fidelity and incomplete inhibition of enzymatic targets at achievable pharmacologic doses in vivo due to half-life, blood–brain barrier and cell permeation, resulting in incomplete and/or heterogeneous access of inhibitors to target populations within the region of injury (An and Fu 2018; Mócsai et al. 2014). As such caution must be utilized when interpreting cell death rate obtained using such reagents. To avoid such complications, we have utilized wildtype and genetic null mutants for caspase-3 and the permeant small molecule inhibitor necrostatin-1 in the current studies.

Through this method, in contrast to the above studies, we observe linked apoptotic-necroptotic neural ischemic cell death response. Specifically, we observe that inhibition of apoptotic and necroptotic response following the induction of cortical ischemic–reperfusion injury is not additive with respect to its protective effects. Rather such blockade was observed to provide comparable levels of neuroprotection to that seen with apoptotic or necroptotic inhibition alone. Importantly, the magnitude of these effects suggests that within the ischemic cortex a substantial population of neurons die through a process of programmed cell death in which the execution of necroptosis and apoptosis within neurons are linked and may operate cooperatively. Consistent with this, we observe that inhibition of RIPK1 phosphorylation results in a marked reduction in TUNEL labeling, a widely utilized marker of apoptosis. Given that TUNEL end-labeling may occur through conditions other than those of classical apoptosis, we utilized several additional cellular and molecular apoptotic markers to identify this form of cell death including activation of the apoptotic executioner caspase-3, -7, and analysis of cellular ultrastructure via electron microscopy. Consistent with the observed RIPK1-mediated diminution of TUNEL labeling, inhibition of RIPK1 also resulted in a substantial reduction in the numbers of ischemic neurons expressing activated caspase-3 and -7 and in the total number of *both* necroptotic and apoptotic cells as determined by electron microscopy. To subsequently distinguish between cell extrinsic mechanisms in which injury promotes (necroptotic) cellular destruction, which results in the release of danger signals triggering subsequent apoptotic cell death, and a cell-intrinsic mechanism in which necroptotic/apoptotic signaling occur within a given cell, we examined the co-expression of RIPK1 and activated caspase-3 in ischemic neurons. Examination of stroke loci revealed marked gradients of $RIPK1^+$ dying neurons confined to zones within several hundred microns of endothelin-1 infusion sites. Analysis of this population reveals the presence of significant numbers of $RIPK1^+$/activated caspase-3^+ double-positive neurons within this ischemic core, consistent with a cell-intrinsic mechanism. These findings thus suggest that the observed effects do not arise as a result of protection of independent populations of necroptotic and apoptotic cells, but rather represent a form of intracellular cooperativity between apoptotic and necroptotic PCD signaling in which RIPK1 activation influence levels of downstream caspase-3/-7 activity.

While reducing overall numbers of dying neurons within the cortex, combinatorial inhibition of caspase-3 and RIPK1 was observed to alter the relative percentage of apoptotic versus necroptotic/necrotic neurons within ischemic sites to values seen in wildtypes, suggesting the presence of alternative or 'sneak' PCD circuits within regions of the injured cortex capable of executing (at least apoptotic) cell death in a RIPK1-independent manner. Based upon the observed pattern of $RIPK1^+$ expression, such regions are likely to exist within more distal (penumbral) regions of cortical injury relative to the site of endothelin-1 infusion. Notably, this RIPK1-independent 'sneak' signaling does not appear to be accessible to wide enough populations of ischemic cortical neurons to provide a functional compensation to PCD levels seen in RIPK1-inhibited versus wildtype animals.

Taken together, these results suggest that RIPK1 activity directly influences the activation of downstream executioner caspases for significant numbers of ischemic neurons. Though such effects may seem surprising, outside the realm of stroke, inhibition of RIPK1 phosphorylation has previously been reported to reduce levels of caspase-3 activation in a model of traumatic brain injury; albeit within tissue extracts for which the nature or location of cells affected could not be definitively established (Wang et al. 2012). Additionally, we have observed similar RIPK1 effects on caspase-3 activation for PCD-activated populations of embryonic stem cells (unpublished data). While the observed cooperative interaction between two traditionally competitive PCD signaling pathways minimally exists within a substantial percentage (~ 50%) of affected ischemic neurons, why such cooperative PCD regulation

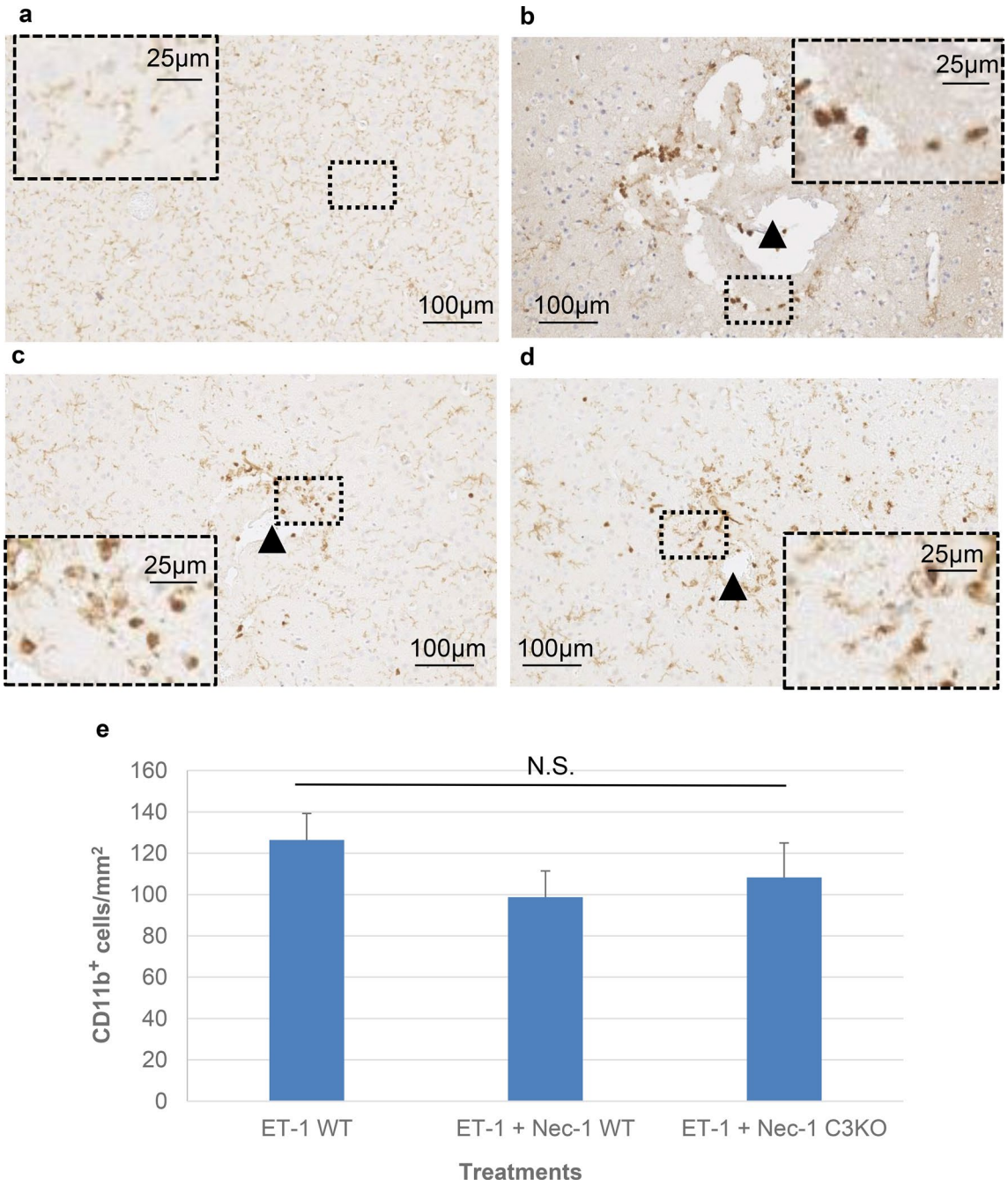

Fig. 5 Distribution of CD11b-positive cells in the brain 24 h post endothelin-1 treatment in wildtype and caspase-3 null mice ± necrostatin-1. Horizontal sections are shown. Black arrowheads indicate relative position of endothelin-1 infusion. **a** Pattern of CD11b staining observed in comparable region and layer of contralateral hemisphere (no endothelin-1 treatment). **b**, **d** Representative examples of distribution of CD11b-positive cells in wildtype (**b**), wildtype exposed to Nec-1 (**c**), and caspase-3 null exposed to nec-1 (**d**) mice. Scale bars as indicated. **e** Counts of CD11b-positive cells/mm^2. Data are represented as mean ± S.E.M. ($n = 12$). Significance determined using a one-way ANOVA with Tukey's Post hoc (F (2, 33) = 0.9076, $p = 0.4133$). *N.S.* not statistically significant at $p < 0.05$

is not uniformly observed in all affected ischemic neurons is presently unknown; however, it may reflect adaptive changes in PCD execution arising as a result of the initial level of ischemic insult.

To gain further insight into the nature of potential inflammatory mediators which may influence the process of PCD execution during the critical first 24 h post ischemia, markers of innate immune response were examined delineating

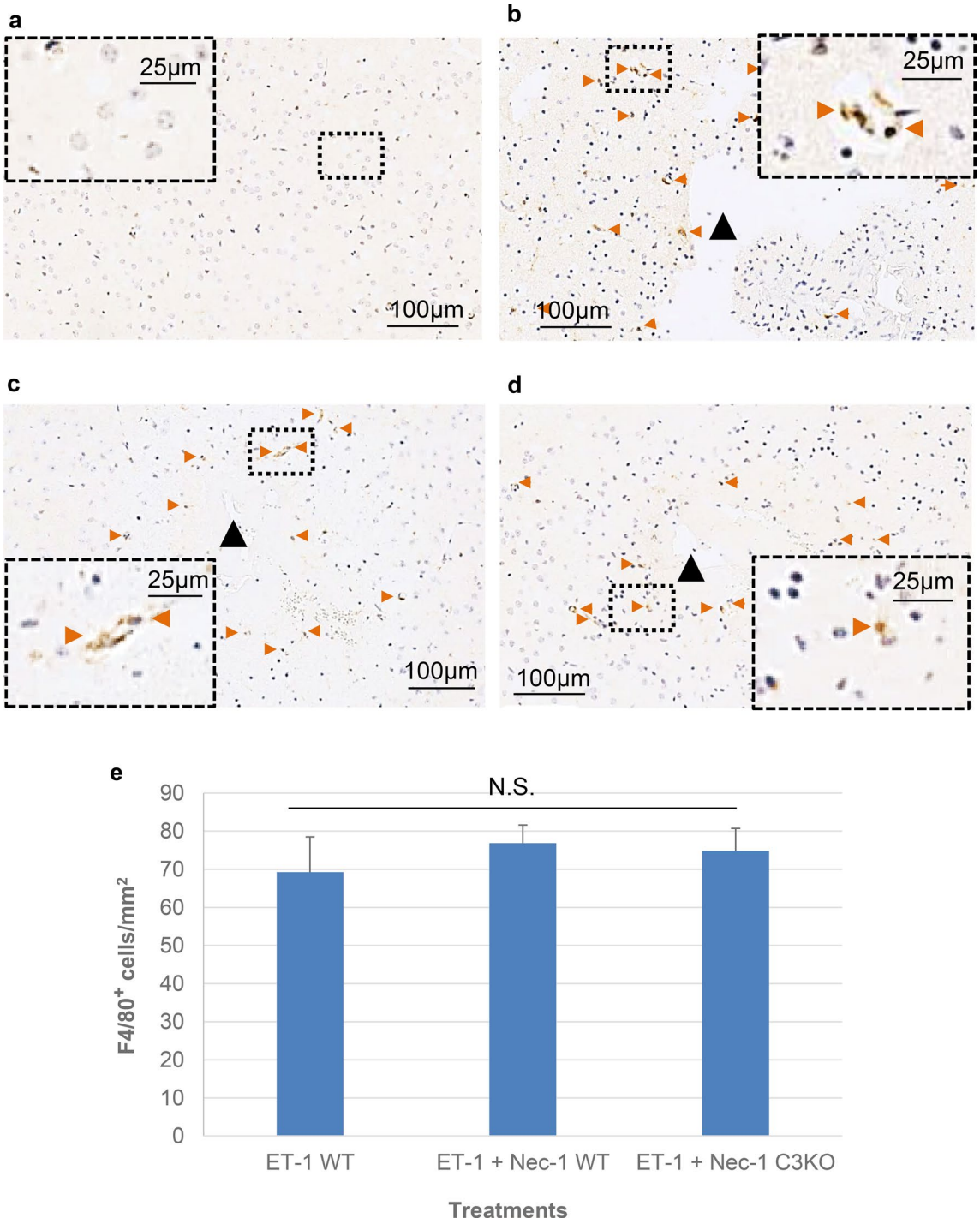

Fig. 6 F4/80 activation in wildtype and caspase-3 null mice exposed to ET-1 with and without necrostatin-1. **a** Representative staining of F4/80 in comparable region and layer of contralateral hemisphere with no endothelin-1 treatment. **b–d** Examples of F4/80-positive cells 24 h post treatment in wildtype (**b**), Nec-1-exposed wildtypes (**c**), and Nec-1-exposed caspase-3 null (**d**) mice. Horizontal sections are shown. Black arrow heads indicate relative position of endothelin-1 infusion. Peroxidase-stained F4/80-positive cells are indicated in each panel by orange arrowheads. Scale for all photomicrographs are as indicated. **e** Counts of F4/80-positive cells/mm^2. Data represented as mean ± S.E.M. ($n = 6$), significance determined using a one-way ANOVA with Tukey's Post hoc (F (2, 15) = 0.2927, $p = 0.7539$). *N.S.* not statistically significant at $p < 0.05$

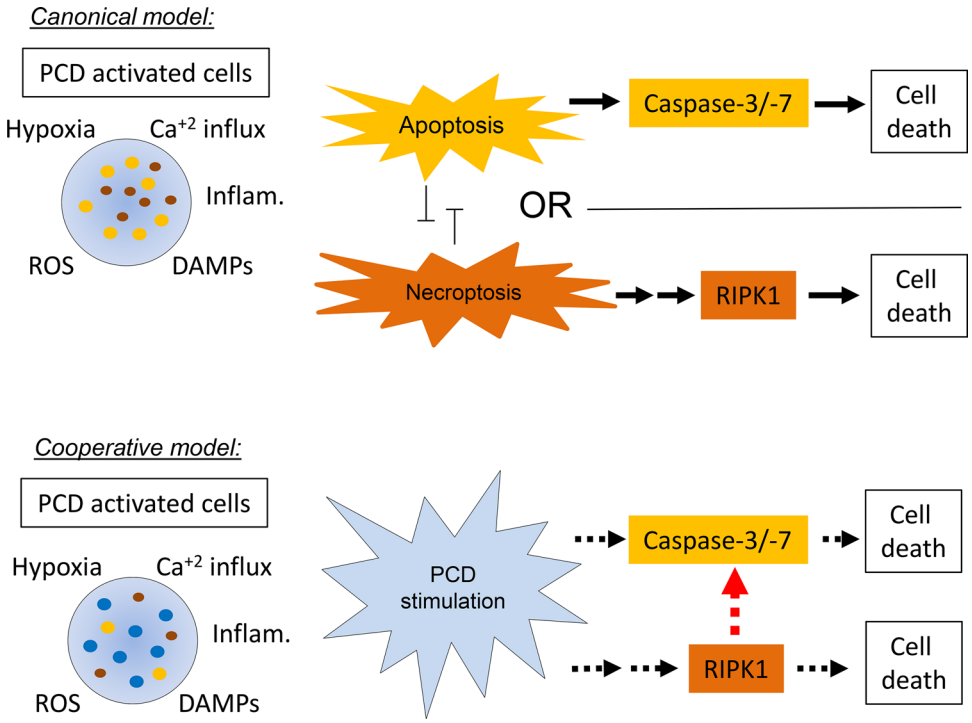

Fig. 7 Schematic cooperative cell death pathway vs. canonical pathway in stroke injury. Traditional/canonical model of ischemic PCD highlights the competitive nature of apoptotic versus necroptotic PCD execution in cells, resulting in independent populations dying by either an apoptotic or necroptotic mechanism. By comparison the cooperative model proposes a role for RIPK1 phosphorylation in enhancing the efficacy of apoptosis via effects on caspase-3/-7 activation (dotted red line). This effect is of sufficient enough strength that it functionally alters the magnitude of isotype-specific cell death (dotted black lines)

populations of granulocytes, monocytes/macrophages, and microglia. Differential staining of CD11b (granulocytes, monocyte/macrophages, microglia marker) (Alliot et al. 1999; Greter et al. 2015; Jeong et al. 2013; Leenen et al. 1994; Prinz et al. 2011) and F4/80 (macrophage/microglial marker) (Alliot et al. 1999; Greter et al. 2015; Prinz et al. 2011) were examined for their distribution. Despite observing differential localization of CD11b and F4/80-positive cells 24 h following endothelin-1 treatment, no significant differences in their distribution or extent were observed between wildtype, Nec-1-treated and Nec-1/caspase-3 knockout groups, further supporting the notion that the effect observed for RIPK1 on executioner caspase activity arises as a result of a direct cell autonomous process.

In summary, the findings observed in this endothelin-1 model of ischemic–reperfusion injury highlight a novel and unexpected relationship between necroptotic and apoptotic signaling in which RIPK1 phosphorylation functionally influences levels of caspase-3/-7 activity based upon the analysis of volumetric, morphologic, cellular, and molecular markers as summarized in Fig. 7. In terms of stroke, these findings suggest that a substantial percentage of ischemic cortical neurons are under the influence of this cooperative signaling during the early stages of CNS injury. This unique necroptotic/apoptotic PCD signaling mode stands in contrast to that observed for many other forms of cellular injury (Han et al. 2011; Lin et al. 1999). Our findings suggest that these effects do not arise as a result of changes in cell-extrinsic inflammatory mediators, but rather as a result of cell-intrinsic signaling. However, the precise molecular mechanisms governing cooperative linkage of RIPK1 phosphorylation to caspase-3/-7 activation are currently unknown and remain to be definitively established in this system.

Acknowledgements We would like to thank Ali Darbandi and William Martin at the Nanoscale Biomedical Imaging Facility at SickKids hospital, Lindsey Fiddes at the University of Toronto for electron microscopy assistance and Lora Stepanian for quantitation assistance.

Author Contributions CDS designed and performed the majority of experiments, analyzed and interpreted the data, and wrote the manuscript; AJE aided with CD11b and F4/80 staining; YC performed animal care; CR, SH, and ACE aided quantitation and analysis; JTH directed the overall study, designed experiments, interpreted the data, and wrote the manuscript.

Funding This study has been funded by grants awarded to J.T.H. from Natural Sciences and Engineering Research Council of Canada (NSERC) (RGPIN 298553-12) and Heart and Stroke Society of Canada (72043506). C.D.S. additionally received scholarship funding from Natural Sciences and Engineering Research Council of Canada (NSERC) and Queen Elizabeth II Graduate Scholarships in Science & Technology—Merck Company of Canada.

Compliance with Ethical Standards

Conflict of interest The authors declare no conflicts of interest.

Ethical Approval All animal experimental procedures were performed in accordance with standards outlined by the Local Animal Care Committee and the University of Toronto, following the guidelines set by Ontario's Animal for Research Act and the federal Canadian Council on Animal Care.

References

Albers GW et al (2016) Ischemic core and hypoperfusion volumes predict infarct size in SWIFT PRIME. Ann Neurol 79:76–89

Alberts B, Johnson A, Lewis J, Raff M, Roberts K, Walter P (2008) Molecular biology of the cell, 5th edn. Garland Science, Taylor and Francis Group, New York

Alliot F, Godin I, Pessac B (1999) Microglia derive from progenitors, originating from the yolk sac, and which proliferate in the brain. Brain Res Dev Brain Res 117:145–152

An S, Fu L (2018) Small-molecule PROTACs: An emerging and promising approach for the development of targeted therapy drugs. EBioMedicine 36:553–562

Bacigaluppi M, Comi G, Hermann DM (2010) Animal models of ischemic stroke. Part two: modeling cerebral ischemia. Open Neurol J 4:34–38

Broughton BR, Reutens DC, Sobey CG (2009) Apoptotic mechanisms after cerebral ischemia. In: Stroke, vol 40. United States, pp e331–e339.

Cai Z et al (2014) Plasma membrane translocation of trimerized MLKL protein is required for TNF-induced necroptosis. Nat Cell Biol 16:55–65

Carmichael ST (2005) Rodent models of focal stroke: size, mechanism, and purpose. NeuroRx 2:396–409

Chen Y, Zhang L, Yu H, Song K, Shi J, Chen L, Cheng J (2018) Necrostatin-1 improves long-term functional recovery through protecting oligodendrocyte precursor cells after transient focal cerebral ischemia in mice. Neuroscience 371:229–241

Cheng YD, Al-Khoury L, Zivin JA (2004) Neuroprotection for ischemic stroke: two decades of success and failure. NeuroRx 1:36–45

Degterev A et al (2005) Chemical inhibitor of nonapoptotic cell death with therapeutic potential for ischemic brain injury. Nat Chem Biol 1:112–119

Del Zoppo GJ, Saver JL, Jauch EC, Adams HP Jr (2009) Expansion of the time window for treatment of acute ischemic stroke with intravenous tissue plasminogen activator: a science advisory from the American Heart Association/American Stroke Association. Stroke 40:2945–2948

Deng X-X, Li S-S, Sun F-Y (2019) Necrostatin-1 prevents necroptosis in brains after ischemic stroke via inhibition of RIPK1-mediated RIPK3/MLKL signaling. Aging Dis 10:807–817

Dojo Soeandy C, Salmasi F, Latif M, Elia AJ, Suo NJ, Henderson JT (2019) Endothelin-1-mediated cerebral ischemia in mice: early cellular events and the role of caspase-3. Apoptosis 24:578–595

Dulli D, D'Alessio DJ, Palta M, Levine RL, Schutta HS (1998) Differentiation of acute cortical and subcortical ischemic stroke by risk factors and clinical examination findings. Neuroepidemiology 17:80–89

Feng S et al (2007) Cleavage of RIP3 inactivates its caspase-independent apoptosis pathway by removal of kinase domain. Cell Signal 19:2056–2067

Ford GA (2008) Clinical pharmacological issues in the development of acute stroke therapies. Br J Pharmacol 153(Suppl 1):S112–119

Fuxe K et al (1992) Involvement of local ischemia in endothelin-1 induced lesions of the neostriatum of the anaesthetized rat. Exp Brain Res 88:131–139

Galluzzi L et al (2018) Molecular mechanisms of cell death: recommendations of the Nomenclature Committee on Cell Death 2018. Cell Death Differ 25:486–541

Ghanavati S, Lerch JP, Sled JG (2014) Automatic anatomical labeling of the complete cerebral vasculature in mouse models. Neuroimage 95:117–128

Gilmour G, Iversen SD, O'Neill MF, Bannerman DM (2004) The effects of intracortical endothelin-1 injections on skilled forelimb use: implications for modelling recovery of function after stroke. Behav Brain Res 150:171–183

Ginsberg MD (2009) Current status of neuroprotection for cerebral ischemia: synoptic overview. Stroke 40:S111–114

Greter M, Lelios I, Croxford AL (2015) Microglia versus myeloid cell nomenclature during brain inflammation. Front Immunol 6:249–249

Han J, Zhong CQ, Zhang DW (2011) Programmed necrosis: backup to and competitor with apoptosis in the immune system. Nat Immunol 12:1143–1149

Heiss WD (2010) The concept of the penumbra: can it be translated to stroke management? Int J Stroke 5:290–295

Hitomi J, Christofferson DE, Ng A, Yao J, Degterev A, Xavier RJ, Yuan J (2008) Identification of a molecular signaling network that regulates a cellular necrotic cell death pathway. Cell 135:1311–1323

Horie N, Maag AL, Hamilton SA, Shichinohe H, Bliss TM, Steinberg GK (2008) Mouse model of focal cerebral ischemia using endothelin-1. J Neurosci Methods 173:286–290

Jeong H-K, Ji K, Min K, Joe E-H (2013) Brain inflammation and microglia: facts and misconceptions. Exp Neurobiol 22:59–67

Jun-Long H et al (2018) Necroptosis signaling pathways in stroke: from mechanisms to therapies. Curr Neuropharmacol 16:1327–1339

Kruidering M, Evan GI (2000) Caspase-8 in apoptosis: the beginning of "the end"? IUBMB Life 50:85–90

Le DA et al (2002) Caspase activation and neuroprotection in caspase-3- deficient mice after in vivo cerebral ischemia and in vitro oxygen glucose deprivation. Proc Natl Acad Sci USA 99:15188–15193

Leenen PJ, de Bruijn MF, Voerman JS, Campbell PA, van Ewijk W (1994) Markers of mouse macrophage development detected by monoclonal antibodies. J Immunol Methods 174:5–19

Lin Y, Devin A, Rodriguez Y, Liu Z-g (1999) Cleavage of the death domain kinase RIP by Caspase-8 prompts TNF-induced apoptosis. Genes Dev 13:2514–2526

Liu C, Zhang K, Shen H, Yao X, Sun Q, Chen G (2018) Necroptosis: a novel manner of cell death, associated with stroke (Review). Int J Mol Med 41:624–630

Macrae IM, Robinson MJ, Graham DI, Reid JL, McCulloch J (1993) Endothelin-1-induced reductions in cerebral blood flow: dose dependency, time course, and neuropathological consequences. J Cereb Blood Flow Metab 13:276–284

McCabe C, Gallagher L, Gsell W, Graham D, Dominiczak AF, Macrae IM (2009) Differences in the evolution of the ischemic penumbra in stroke-prone spontaneously hypertensive and Wistar-Kyoto rats. Stroke 40:3864–3868

Meng X, Fisher M, Shen Q, Sotak CH, Duong TQ (2004) Characterizing the diffusion/perfusion mismatch in experimental focal cerebral ischemia. Ann Neurol 55:207–212

Mócsai A, Kovács L, Gergely P (2014) What is the future of targeted therapy in rheumatology: biologics or small molecules? BMC Med 12:43

Nair P, Lu M, Petersen S, Ashkenazi A (2014) Chapter five-apoptosis initiation through the cell-extrinsic pathway. In: Ashkenazi A, Yuan J, Wells JA (eds) Methods in enzymology. Academic Press, San Diego, pp 99–128

Pan B et al (2014) C-Abl tyrosine kinase mediates neurotoxic prion peptide-induced neuronal apoptosis via regulating mitochondrial homeostasis. Mol Neurobiol 49:1102–1116

Pan Y et al (2015) STI571 protects neuronal cells from neurotoxic prion protein fragment-induced apoptosis. Neuropharmacology 93:191–198

Prinz M, Priller J, Sisodia SS, Ransohoff RM (2011) Heterogeneity of CNS myeloid cells and their roles in neurodegeneration. Nat Neurosci 14:1227

Pulli B et al (2012) Acute ischemic stroke: infarct core estimation on CT angiography source images depends on CT angiography protocol. Radiology 262:593–604

Radak D et al (2017) Apoptosis and acute brain ischemia in ischemic stroke. Curr Vasc Pharmacol 15:115–122

Raghupathi R (2004) Cell death mechanisms following traumatic brain injury. Brain Pathol 14:215–222

Raghupathi R, Graham DI, McIntosh TK (2000) Apoptosis after traumatic brain injury. J Neurotrauma 17:927–938

Roome RB, Bartlett RF, Jeffers M, Xiong J, Corbett D, Vanderluit JL (2014) A reproducible Endothelin-1 model of forelimb motor cortex stroke in the mouse. J Neurosci Methods 233:34–44

Sakai R, Henderson JT, O'Bryan JP, Elia AJ, Saxton TM, Pawson T (2000) The mammalian ShcB and ShcC phosphotyrosine docking proteins function in the maturation of sensory and sympathetic neurons. Neuron 28:819–833

Sapira V, Cojocaru IM, Lilios G, Grigorian M, Cojocaru M (2010) Study of endothelin-1 in acute ischemic stroke. Roman J Internal Med 48:329–332

Schug ZT, Gonzalvez F, Houtkooper RH, Vaz FM, Gottlieb E (2011) BID is cleaved by caspase-8 within a native complex on the mitochondrial membrane. Cell Death Differ 18:538–548

Simonetti G et al (2013) Endovascular management of acute stroke. J Cardiovasc Surg (Torino) 54:101–114

Soylu H, Zhang D, Buist R, Martin M, Albensi BC, Parkinson FE (2012) Intracortical injection of endothelin-1 induces cortical infarcts in mice: effect of neuronal expression of an adenosine transporter. Exp Transl Stroke Med 4:4

Sun Y, Xu Y, Geng L (2015) Caspase-3 inhibitor prevents the apoptosis of brain tissue in rats with acute cerebral infarction. Exp Ther Med 10:133–138

Symon L (1987) Recovery of brain function after ischaemia. Acta Neurochir Suppl (Wien) 41:97–103

Takahashi N et al (2012) Necrostatin-1 analogues: critical issues on the specificity, activity and in vivo use in experimental disease models. Cell Death Dis 3:e437

Tennant KA, Jones TA (2009) Sensorimotor behavioral effects of endothelin-1 induced small cortical infarcts in C57BL/6 mice. J Neurosci Methods 181:18–26

Vanlangenakker N, Vanden Berghe T, Krysko DV, Festjens N, Vandenabeele P (2008) Molecular mechanisms and pathophysiology of necrotic cell death. Curr Mol Med 8:207–220

Wang YQ et al (2012) Necrostatin-1 suppresses autophagy and apoptosis in mice traumatic brain injury model. Neurochem Res 37:1849–1858

Wiley KE, Davenport AP (2004) Endothelin receptor pharmacology and function in the mouse: comparison with rat and man. J Cardiovasc Pharmacol 44(Suppl 1):S4–6

Windle V, Szymanska A, Granter-Button S, White C, Buist R, Peeling J, Corbett D (2006) An analysis of four different methods of producing focal cerebral ischemia with endothelin-1 in the rat. Exp Neurol 201:324–334

Woo M et al (1998) Essential contribution of caspase 3/CPP32 to apoptosis and its associated nuclear changes. Genes Dev 12:806–819

World Health Organization (2004) Global burden of stroke. https://www.who.int/cardiovascular_diseases/en/cvd_atlas_15_burden_stroke.pdf. Accessed 4 May 2016

Xu X, Chua KW, Chua CC, Liu CF, Hamdy RC, Chua BH (2010) Synergistic protective effects of humanin and necrostatin-1 on hypoxia and ischemia/reperfusion injury. Brain Res 1355:189–194

Yuan J (2009) Neuroprotective strategies targeting apoptotic and necrotic cell death for stroke. Apoptosis 14:469–477

Zgavc T, Ceulemans AG, Hachimi-Idrissi S, Kooijman R, Sarre S, Michotte Y (2012) The neuroprotective effect of post ischemic brief mild hypothermic treatment correlates with apoptosis, but not with gliosis in endothelin-1 treated rats. BMC Neurosci 13:105

Zhang S, Wang Y, Li D, Wu J, Si W, Wu Y (2016) Necrostatin-1 attenuates inflammatory response and improves cognitive function in chronic ischemic stroke mice. Medicines (Basel) 3:16